https://doi.org/10.5607/en22013
Exp Neurobiol. 2022 Aug;31(4):243-259.
pISSN 1226-2560 • eISSN 2093-8144

Original Article

Experimental Neurobiology

# Low-voltage Activating $K^+$ Channels in Cochlear Afferent Nerve Fiber Dendrites

**Kushal Sharma[1], Kwon Woo Kang[1], Young-Woo Seo[2], Elisabeth Glowatzki[3] and Eunyoung Yi[1]***

*[1]College of Pharmacy and Natural Medicine Research Institute, Mokpo National University, Muan 58554, [2]KBSI Gwangju Center, Korea Basic Science Institute, Gwangju 61186, Korea, [3]Department of Otolaryngology-Head and Neck Surgery and Neuroscience, The Johns Hopkins School of Medicine, Baltimore, MD 21205, USA*

Cochlear afferent nerve fibers (ANF) are the first neurons in the ascending auditory pathway. We investigated the low-voltage activating $K^+$ channels expressed in ANF dendrites using isolated rat cochlear segments. Whole cell patch clamp recordings were made from the dendritic terminals of ANFs. Outward currents activating at membrane potentials as low as -64 mV were observed in all dendrites studied. These currents were inhibited by 4-aminopyridine (4-AP), a blocker known to preferentially inhibit low-voltage activating $K^+$ currents ($I_{KL}$) in CNS auditory neurons and spiral ganglion neurons. When the dendritic $I_{KL}$ was blocked by 4-AP, the EPSP decay time was significantly prolonged, suggesting that dendritic $I_{KL}$ speeds up the decay of EPSPs and likely modulates action potentials of ANFs. To reveal molecular subtype of dendritic $I_{KL}$, α-dendrotoxin (α-DTX), a selective inhibitor for $K_v1.1$, $K_v1.2$, and $K_v1.6$ containing channels, was tested. α-DTX inhibited 23±9% of dendritic $I_{KL}$. To identify the α-DTX-sensitive and α-DTX-insensitive components of $I_{KL}$, immunofluorescence labeling was performed. Strong $K_v1.1$- and $K_v1.2$-immunoreactivity was found at unmyelinated dendritic segments, nodes of Ranvier, and cell bodies of most ANFs. A small fraction of ANF dendrites showed $K_v7.2$-immunoreactivity. These data suggest that dendritic $I_{KL}$ is conducted through $K_v1.1$and $K_v1.2$ channels, with a minor contribution from $K_v7.2$ and other as yet unidentified channels.

**Key words:** Cochlea, $K_v1.1$, $K_v1.2$, Auditory nerve fiber, Hair cell, Ribbon synapse

## INTRODUCTION

Neurons in the auditory pathway are characterized by the ability to detect small differences in the timing of incoming signals. For example, auditory brainstem neurons process interaural time differences as brief as 100 μs and use this information to determine sound locations [1]. To fulfil their role in sound information processing auditory neurons need to fire brief, well-timed action potentials (APs) at high rates, and their AP time course and shape is significantly regulated by $K^+$ currents. Most neurons in auditory nuclei express high- ($I_{KH}$) and low-voltage activating $K^+$ currents ($I_{KL}$), although cell type-dependent variabilities in the size, density, and kinetics of these $K^+$ currents are present [2-4]. Pharmacological and gene knock-out studies have demonstrated that $I_{KH}$ and $I_{KL}$ in brainstem auditory neurons are predominantly conducted by members of the $K_v3$ and $K_v1$ families of $K^+$ channels, respectively [2-6]. $I_{KH}$ facilitates the repolarization of APs and shortening of AP duration, while $I_{KL}$ is partially active near the resting potential of auditory neurons and decreases the membrane time constant at rest and during synaptic stimulation. Thus, $I_{KL}$ plays a significant role in shortening EPSPs and APs, thereby minimizing temporal variability in AP firing and preventing aberrant AP generation.

$K^+$ currents in auditory neurons might undergo developmental changes. A patch-clamp study on rat calyx of Held reported that both TEA-sensitive $I_{KH}$ and margatoxin-sensitive $I_{KL}$ exhibited about 3-fold increase in amplitude and 2~3-fold acceleration in

Submitted April 1, 2022, Revised June 18, 2022,
Accepted July 29, 2022

*To whom correspondence should be addressed.
TEL: 82-61-450-2683, FAX: 82-61-450-2689
e-mail: eunyoungyi@mokpo.ac.kr

the activation kinetics from postnatal day 7 (P7) to P14 [7]. Similarly, in gerbil medial superior olive (MSO) principal neurons a 390% increase in $I_{KL}$ was reported from P14 to P21 [8]. Over the same period, relative proportion of dendrotoxin-K (DTX-K)-sensitive current in the MSO neuron $I_{KL}$ also increased from 76% to 91%. However, no such developmental change was found in medial nucleus of the trapezoid body (MNTB) neurons. In rat cochlear nucleus neurons mRNA and protein levels of $K_v1.1$, $K_v1.2$, and $K_v3.1$ increased during first 3 postnatal weeks and reached a stable state afterward while $K_v4.2$ expression gradually decreased from postnatal to the young adult ages [9]. These findings indicated that developmental refinement of $K^+$ currents in auditory synapses could occur in cell type- and channel subtype-specific manner.

ANFs are bipolar neurons with unmyelinated dendritic ending at the hair cell ribbon synapse and myelinated peripheral and central processes and soma. They conduct signals from sensory hair cells to neurons in the cochlear nucleus of the brainstem [10], achieving a high temporal precision of synaptic transmission by mechanisms similar to those of neurons in auditory nuclei. Well-timed AP firing of ANFs with minimal latency and jitter is regulated by several factors including the occurrence of large and brief excitatory postsynaptic currents (EPSCs), and AP generator regions located near the IHC- ANF synapses [11-15]. In addition, investigations of the cell bodies of ANFs (also known as the spiral ganglion neurons; SGNs) revealed expression of multiple $K^+$ channel types, including $K_v3$ and $K_v1$ [16-20]. Recordings from isolated SGN somata indicated that active electrical properties such as resting membrane potential, AP threshold and AP firing pattern are finely tuned by different combinations of $K^+$ currents along with other ionic currents. It remains to be clarified whether the classes of $K^+$ channels found in SGN somata are present in the unmyelinated ANF endings contacting IHCs and if they exert similar effects on AP generation of ANFs [13].

It has been demonstrated that ANF dendrites exhibit various ion channels including hyperpolarization-activated, cyclic nucleotide-gated (HCN), voltage-gated $Na^+$, $I_{KH}$ and $I_{KL}$ [21]. Here, we further investigated the electrical properties, subunit composition, and physiological role of $K^+$ currents in ANF dendrites. We confirmed the presence of a 4-AP-sensitive $I_{KL}$ in ANF dendritic terminals, demonstrated its physiological role in dendritic excitatory postsynaptic potentials (EPSPs) using patch clamp recordings, and identified the classes and locations of $K^+$ channels conducting $I_{KL}$ using subtype selective $K^+$ channel blockers and immunolabeling with specific antibodies to particular $K^+$ channel subunits.

## MATERIALS AND METHODS

All animal procedures were performed in accordance with animal protocols approved by the Johns Hopkins University Animal Care and Use Committee and Mokpo National University Institutional Animal Care and Use Committees. All experiments were performed using excised cochlear turns dissected from Sprague Dawley rats euthanized by an overdose of isoflurane or sevoflurane inhalation, followed by decapitation. Then, cochleae were quickly dissected free in standard external solution.

### *Electrophysiological recordings*

Whole cell patch clamp recordings from the cell body or dendritic terminal of cochlear afferent nerve fiber was performed as described previously [21, 22]. Excised apical cochlear turns from 1 day (for spiral ganglion neuron recordings) or 7~14 day-old rats (for ANF dendritic recordings) were placed in a chamber under an upright microscope (Axioskop2 FS plus, Zeiss) and superfused with external solution at 1~3 ml/minute. IHCs and contacting ANF dendrites were visualized on a monitor via a 40× water immersion objective, 4× magnification, Normaski optics and a NC 70 Newvicon camera (Dage). The standard external solution was (in mM): 5.8 KCl, 155 NaCl, 1.3 $CaCl_2$, 0.9 $MgCl_2$, 0.7 $NaH_2PO_4$, 5.6 Glucose, 10 HEPES; 300 mOsm, pH 7.4 (NaOH). The pipette solution was (in mM): 135 KCl, 3.5 $MgCl_2$, 0.1 $CaCl_2$, 5 EGTA, 5 HEPES, 0~2.5 $Na_2ATP$; or 135 KCl, 3.5 $MgCl_2$, 0.1 $CaCl_2$, 5 EGTA, 5 HEPES, 4 $Na_2ATP$, 0.2 Na GTP; 290 mOsm, pH 7.2 (KOH). Liquid junction potentials (4 mV) were corrected off-line. Drugs were dissolved in external solution to their final concentrations from frozen stocks daily. Drug solutions were applied using a gravity-driven flow pipette (100 μm tip diameter) placed near the recording site, connected to a VC-6 channel valve controller (Warner Instrument). ZD7288, 6-cyano-7-nitroquinoxaline-2,3-dione (CNQX), 4-AP were purchased from Tocris Bioscience, α-DTX from Alomone Labs and tetrodotoxin (TTX) from either Alomone Labs or Sigma. All other chemicals were purchased from Sigma.

Recording pipettes were pulled with a multi-step horizontal puller (P97, Sutter), using 1 mm borosilicate glass (1B100F-4, WPI), fire-polished (MF200, WPI, final tip resistance 10~15 MΩ), and coated with Sylgard® (Dow Corning). Recordings were performed at 22~25℃ using a Multiclamp 700A or 700B amplifier (Molecular Devices), pClamp version 9.2 software, and a Digidata 1322A board, digitized at 50 kHz and filtered at 10 kHz. In voltage-clamp mode, series resistance ($R_s$) was estimated from capacitative currents in response to 10 mV voltage steps (-84 to -94 mV) [21]. Data were discarded if $R_s$ >50 MΩ. In current-clamp mode, errors



https://doi.org/10.5607/en22013

**Table 1.** Primary antibodies used in this study

| Antigen | Host | Supplier | Catalog number | Dilution |
|---|---|---|---|---|
| $K_v1.1$ | Mouse monoclonal | Neuromab | 75-105 | 1:500 |
| $K_v1.2$ | Mouse monoclonal | Neuromab | 73-008 | 1:200 |
| $K_v7.2$ | Rabbit polyclonal | Abcam | Ab22897 | 1:500 |
| $K_{2p}2.1$ | Rabbit polyclonal | Alomone labs | APC-047 | 1:500 |
| Calretinin | Mouse monoclonal | Millipore | MAB1568 | 1:500 |
| Calretinin | Rabbit polyclonal | Millipore | AB5054 | 1:500 |
| Parvalbumin | Goat polyclonal | Swant | PVG-213 | 1:500 |
| $Na^+, K^+$- ATPase | Mouse monoclonal | Thermo Scientific | MA3-915 | 1:500 |
| $Na^+, K^+$- ATPase | Goat polyclonal | Santa Cruz Biotechnology | sc-16052 | 1:500 |
| Caspr-2 | Rabbit polyclonal | US Biological | C7865-2 | 1:500 |
| Neurofilament H | Chicken polyclonal | Millipore | AB5539 | 1:1,000 |

due to $R_s$ were compensated using the bridge balance and pipette capacitance neutralization. To avoid results from damaged cells we excluded data from cells exhibiting membrane potential -40 mV or less negative in current clamp mode or holding current larger than -200 pA at holding potential -84 mV in voltage clamp mode. Average resting potential of the cells included in current study was -67.2±4.0 mV in our standard external solution. Data were analyzed off-line using pClamp version 9.2 or 10.5 (Molecular Devices), MiniAnalysis (Synaptosoft) and Origin 7.5 (OriginLab). For statistical comparisons Sigmaplot12 (SYSTAT Software Inc.) was used. Statistical significance of irreversible drug effects (α-DTX) was tested using a paired-t-test. Effects of reversible drugs (4-AP and TEA) were tested using one-way repeated measures analysis of variance (RM ANOVA) followed by Student-Newman-Keuls test. $p<0.05$ is considered to be statistically significant. Values are presented as mean±standard deviations (S. D.).

### *Immunohistochemistry*

The methods for cochlear tissue preparation and imaging was adapted from the procedure described previously [23, 24]. Cochleae were quickly collected from postnatal (P9, P15-21) Sprague Dawley rats and immediately perfused through either the oval or round windows with ice cold paraformaldehyde (4%) or formaldehyde (4%) prepared in phosphate buffered saline (PBS; pH 7.4). Cochleae were then kept in the fixative for 1 h at 4℃ and then rinsed with PBS for 3 times. Apical turns of the cochleae were carefully separated, immersed in blocking buffer (PBS containing 5% donkey or goat serum and 0.25% Triton-X-100) for 1 h at room temperature, then incubated in primary antibody diluted with blocking buffer overnight at 4℃. The next day, tissues were washed 3 times with blocking buffer (20 min each) then incubated with fluorescence tagged secondary antibodies diluted in blocking buffer for 1 h at room temperature. The tissues were then washed once in blocking buffer (20 min), and twice in PBS (10 min), then mounted on glass slides using Fluorsave® mounting medium (Calbiochem, 345789). Tissue images were obtained using Laser Scanning Confocal Microscope (Leica TCS SP5/AOBS/Tandem at the Korea Basic Science Institute, Gwangju Center or Zeiss LSM 710 at Mokpo National University). Confocal z-stacks were collected at 0.3~0.99 μm interval. Image analyses and reconstructions were carried out using image viewing software provided by the microscope manufacturers (Zeiss Zen or Leica LAS AF lite), Imaris (version 7.3.0, Bitplane, Switzerland)) and ImageJ (NIH). No labeling was observed when the primary antibodies were omitted.

The primary antibodies used in this study are listed in Table 1. Donkey anti-chicken secondary antibody conjugated with Alexa Fluor 647 was purchased from Millipore (AP194SA6, 1:1,000). All other secondary antibodies (Alexa Fluor 488, 555, and 633 generated in either goat or donkey) were purchased from Molecular Probes/Invitrogen and used at 1:1,000.

### *Quantification of colocalization*

To quantify the co-localization for $K_v1.1$, $K_v1.2$ and NKA, the confocal 3D data sets were imported and reconstructed with Imaris software for visualization and volume rendering. Co-localization analysis was performed with ImarisColoc module of the Imaris software, which provides statistical parameters that include the number of co-localized voxels, the Manders' coefficient. The Manders' coefficient values of co-localized voxels from two acquired channels were measured via built-in automated background threshold determination of ImarisColoc module.

Manders' coefficients are calculated as:

$$M1 = \frac{\Sigma A_{i,colocal}}{\Sigma A_i}$$

Where $A_{i,colcoal} = A_i$ if $B_i > 0$ and $A_{i,colocal} = 0$ if $B_i = 0$ and

$$M2 = \frac{\Sigma B_{i,colocal}}{\Sigma B_i}$$

Where $B_{i,colocal} = B_i$ if $A_i > 0$ and $B_{i,colocal} = 0$ if $A_i = 0$

A: signal intensity of NKA labeling, B: signal intensity of $K_v1.1$ or $K_v1.2$ labeling

The Manders' coefficient values range from 0 to 1; the value 1 indicating the total signal from one channel completely overlapping with the signal from the other.

## RESULTS

### *High- and low-voltage activating $K^+$ currents of ANF dendrites*

Our previous work demonstrated that nearly all rat ANF dendrites expressed $I_{KH}$ and $I_{KL}$ [21]. In this study we used whole-cell patch clamp recordings to further analyze these dendritic $K^+$ currents during pharmacological blockade of dendritic $Na^+$, $Ca^{2+}$, HCN and AMPA receptor-mediated synaptic currents with 1~2 μM TTX, 200 μM $CdCl_2$, 50 μM ZD7288 and 10 μM CNQX, respectively. The remaining outward currents were evoked by voltage steps (10 mV, 200 ms, holding potential -84 mV) from -104 mV to +36 mV, and tested for their sensitivity to the $K^+$ channel blockers tetraethylammonium (TEA) and 4-aminopyridine (4-AP) (Fig. 1). In many neurons in auditory pathway, TEA preferentially inhibited $I_{KH}$ while 4-AP exhibited more selectivity to $I_{KL}$ [2, 3, 25, 26]. TEA slightly reduced the outward currents at test potentials below -34 mV and significantly altered the current-voltage relationship (Fig. 1A, B) at test potentials between -24 and +36 mV, resulting in a steeper growth of the TEA-sensitive currents (Fig. 1B, G; n=4, $p<0.05$). These data indicated that ANF dendrites possessed a TEA-sensitive $I_{KH}$ activating around -24 mV in addition to a small TEA-sensitive $I_{KL}$ component.

The inhibitory effects of 4-AP (Fig. 1C) were greatest during the first 20 ms of voltage steps (dotted vertical lines) and currents were significantly decreased from control at test potentials between -44 mV and +36 mV (Fig. 1D, n=8, $p<0.05$). In contrast, the contribution of 4-AP-resistant currents increased noticeably during voltage steps positive to -34 mV, consistent with the previously described activation of $I_{KH}$ [2, 27]. The 4-AP-resistant currents were significantly inhibited by a combination of 4-AP and TEA at test potentials between -24 mV and +36 mV (Fig. 1E, F). Taken together, $I_{KH}$ were more effectively blocked by TEA while $I_{KL}$ appeared more sensitive to 4-AP despite some degree of overlap in their voltage range.

### *$I_{KL}$ shortens synaptic potential duration at the IHC-ANF synapse*

Current-voltage plots revealed that dendritic $I_{KL}$ was activated within the voltage range in which EPSPs operate at the IHC-ANF synapse (-65 to -30 mV) [21]. Since activation of $I_{KL}$ has been shown to affect EPSPs in CNS auditory neurons [28-30], we tested the effects of blocking $I_{KL}$ with 4-AP on EPSPs (Fig. 2A~C). In the presence of 4-AP (4 mM), EPSP time constants of decay ($\tau_{decay}$) were significantly increased by 22±7% (from 5.5±1.9 ms to 6.7±2.2 ms, n=5 in 15 mM $K^+$, n=1 in 5.8 mM $K^+$ extracellularly, 2248 EPSPs analyzed, $p<0.01$) compared to control, and this effect was reversed to 112±13% of control (5.33±1.18 ms, n=3; Fig. 2A) upon washout. The changes in $\tau_{decay}$ caused by 4-AP were similar over the wide range of EPSP amplitudes. EPSP rise times (10%~90%; 1.20±0.37 vs. 1.29±0.52 ms, p=0.801), EPSP amplitudes (13.3±6.3 mV vs. 12.8±6.1 mV, p=0.411), and ANF dendritic membrane potentials were all unaffected by 4-AP (55.1±13.1 mV to 55.3±13.5mV, p=0.551). Synaptic EPSCs were unaffected by 4-AP (10~90% rise times; 0.36±0.08 vs. 0.32±0.10 ms, p=0.558; $\tau_{decay}$, 1.05±0.09 vs. 1.11±0.30 ms, p=0.801, n=3, 380 EPSCs analyzed), excluding unspecific effects of the drug presynaptically or on glutamate receptors. Thus, we concluded that activation of $I_{KL}$ in ANF dendrites shortened EPSP durations over the physiological range of EPSP amplitudes.

### *α-DTX-sensitive $K^+$ channels mediate a part of dendritic $I_{KL}$*

We proceeded to further analyze $I_{KL}$ because it was significantly activated in the voltage range of dendritic EPSPs. In SGNs and auditory neurons of the cochlear nucleus, 4-AP-sensitive currents also exhibited a sensitivity to α-DTX [2, 20], which irreversibly blocks $K^+$ channels containing $K_v1.1$, 1.2, or 1.6 subunits [31]. To test dendritic $I_{KL}$ in ANFs for sensitivity to α-DTX, we compared the outward currents before and during α-DTX application (Fig. 3A~E). Unlike results in SGNs α-DTX inhibited only a small part of dendritic $I_{KL}$. We measured the amplitudes of outward currents evoked by repeated voltage steps (0.1 Hz, 200 ms) from -84 to -34 mV (a voltage step activating significant $I_{KL}$ but minimal $I_{KH}$) before and during α-DTX application (Fig. 3C, D). We often observed a significant rundown of outward currents during these experiments. Therefore, in these recordings, current amplitudes in the presence of α-DTX were statistically compared to extrapolated control values calculated from a linear fit of currents recorded during a control period (Fig. 3D, blue line). α-DTX (100~200 nM) reduced the outward currents by 23±9% (Fig. 3E, from 84±41 to 64±29 pA, n=6, $p<0.05$). The α-DTX sensitivity of dendritic $I_{KL}$ differed markedly from results in cultured mouse SGN somata [20], where α-DTX caused a near complete block of $I_{KL}$. Therefore, we compared the α-DTX sensitivity of $I_{KL}$ from acutely excised SGN somata (Fig. F~J). No rundown of the outward current amplitudes was observed (Fig. 3I) and α-DTX inhibited 90±2% of the outward


https://doi.org/10.5607/en22013

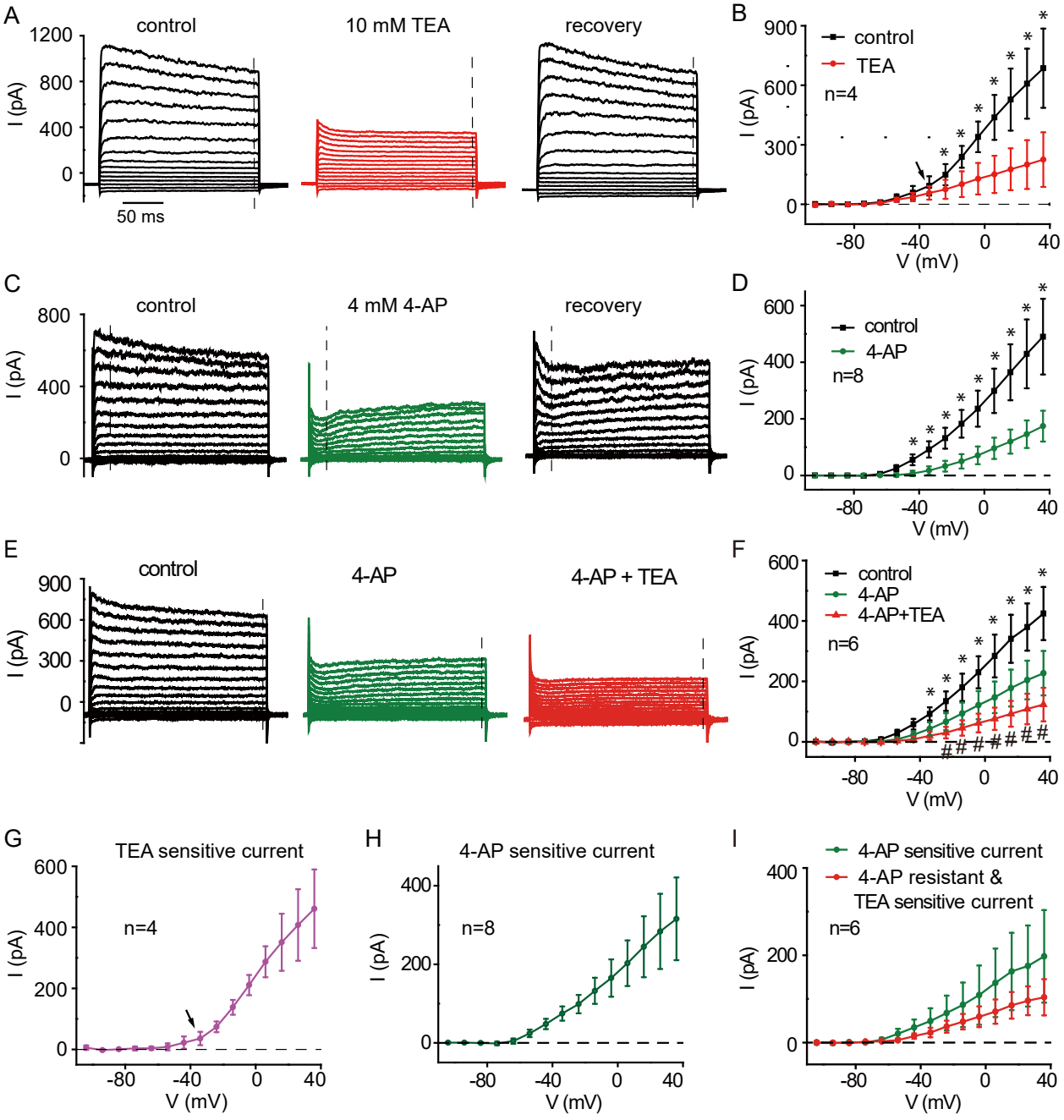


**Fig. 1.** Sensitivity of $K^+$ currents to TEA and 4-AP. (A, C, E) Current responses to 200 ms voltage steps before, during and after application of 10 mM TEA and/or 4 mM 4-AP. Voltage steps from -104 to +36 mV in 10 mV increments, from a holding potential of -84 mV. External solution contained TTX (1 μM), $CdCl_2$ (200 μM), ZD7288 (50 μM), and CNQX (10 μM). (B, D, F) Current voltage relations with and without TEA and/or 4-AP (mean±S.D.) after leak subtraction. Current amplitudes were measured at the time marked by vertical dotted lines (20 or 195 ms into the voltage steps). (G) The TEA sensitive current was calculated as the difference of currents measured in control and TEA as shown in B. (H) The 4-AP sensitive current was calculated as the difference of currents measured in control and 4-AP as shown in D. (I) The 4-AP sensitive and the 4-AP resistant and TEA sensitive currents were calculated as the difference of currents measured in control, 4-AP, and 4-AP + TEA as shown in F. A change in the steepness of the functions in B and G (arrows) suggests two components of TEA sensitive current. *Significant difference between control vs. TEA or control vs 4-AP. #Significant difference between 4-AP vs. 4-AP+TEA.

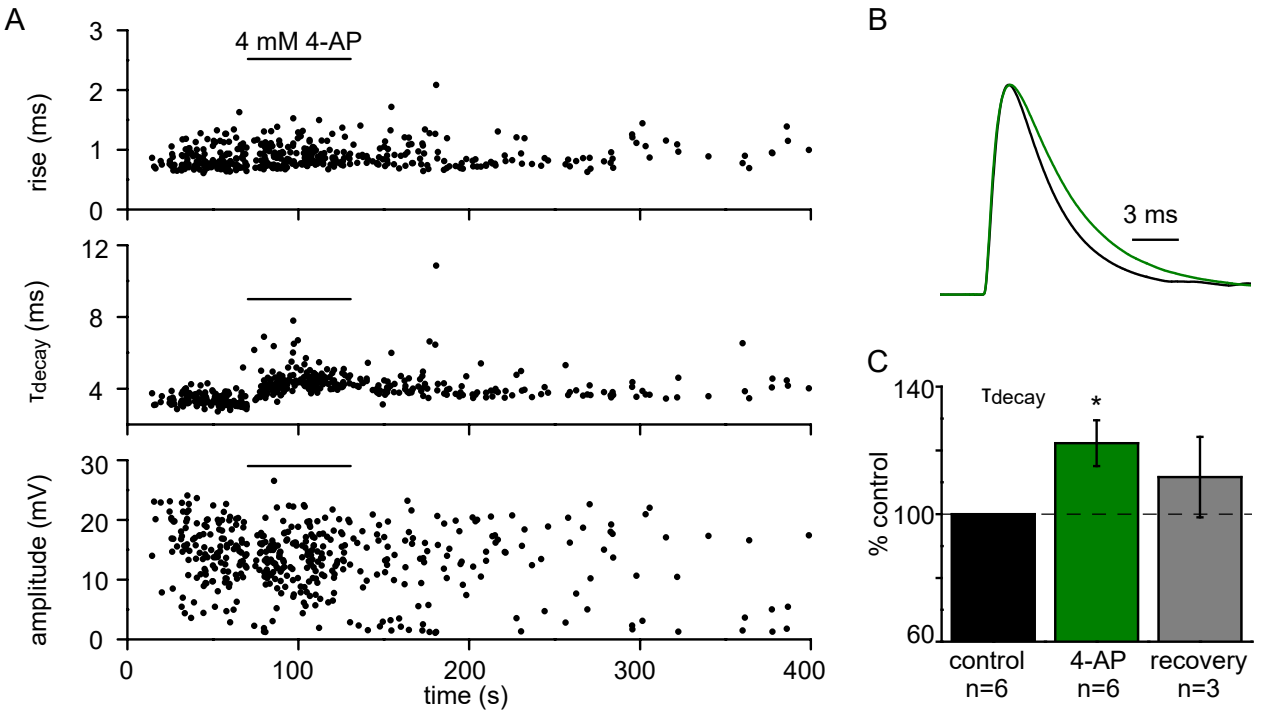


**Fig. 2.** $I_{KL}$ shorten EPSPs in afferent dendrites. (A) EPSP waveform parameters were monitored (1 μM TTX) before, during and after blocking $I_{KL}$ with 4 mM 4-AP. 10~90% EPSP rise time (rise), EPSP decay time constant ($\tau_{decay}$) and EPSP amplitude. Resting membrane potential before, during and after 4-AP application was -52.4 mV, -52.2 mV and -52.3 mV, respectively. (B) normalized average EPSP waveforms before and after block of $I_{KL}$ with 4-AP for experiment in A. control: $\tau_{decay}$=3.39 ms (black, average of 138 EPSPs), in 4 mM 4-AP: $\tau_{decay}$=4.46 ms (green, average of 43 EPSPs). (C) Summarized results for 6 recordings. *Significant difference between control vs. 4-AP.

current (Fig. 3J, from 95±18 to 9±2 pA, n=3, p<0.001). These results suggested that, based on α-DTX sensitivity, the low-voltage activated $K^+$ channel population in the dendrites differed from that in the somata of ANFs. The differences in α-DTX-sensitivity between dendrites and the cell bodies are not likely due to age difference. Patch-clamp recordings of SGNs isolated from animals of more advanced age consistently reported that $I_{KL}$ of SGN cell bodies were predominantly inhibited by dendrotoxins [18, 20, 32]. Considering that ANF dendrites are the primary site of lateral olivocochlear (LOC) innervation, the possibility that certain LOC neurotransmitters might modulate ANF activities by modifying dendritic ion channels has long been postulated. Expression of a variety of dendritic $K^+$ channels would increase the chance of forming diverse LOC neurotransmitter-ion channel partnerships, which could produce case-by-case fine-tuning of synaptic potentials when they are first generated.

### *Most ANF dendrites express $K_v$1.1 and $K_v$1.2 subunits*

We next studied the molecular identities and cellular locations of dendritic $K^+$ channels conducting $I_{KL}$ using immunofluorescence labeling with $K^+$ channel subtype-specific antibodies.

Our pharmacological data indicated that an α-DTX-sensitive $K^+$ channel subtype contributed to $I_{KL}$ in ANF dendrites, and functional expression of the α-DTX-sensitive subtypes $K_v$1.1 and $K_v$1.2 has been demonstrated in SGN somata [16, 19]. Therefore, we tested for $K_v$1.1- and $K_v$1.2-immunoreactivity of the dendritic terminals of ANFs. Although $K_v$1.6 is also sensitive to α-DTX we did not further pursuit $K_v$1.6 here. Transcriptomic studies on dissociated mouse SGNs reported that $K_v$1.6 expression was restricted to a small population of SGNs, especially to the ones innervating OHCs whereas transcripts for $K_v$1.1 and $K_v$1.2 were found in most, if not all, SGNs [33-35]. To reveal the cellular location of $K_v$1.1- or $K_v$1.2-immunolabed structures, we co-labeled tissues with known cellular markers. Parvalbumin and calretinin are $Ca^{2+}$- buffering proteins found in hair cell and ANFs. $Na^+$, $K^+$-ATPase (NKA) and neurofilament heavy (NFH) are found in the unmyelinated dendritic segment and the peripheral process of type 1 ANFs, respectively [36-38]. As expected from the α-DTX-sensitivity, low magnification images revealed $K_v$1.1-immunoreactivity in the IHC region and spiral ganglia region (Fig. 4A~F). High magnification confocal images of IHC regions revealed that $K_v$1.1-immunoreactivity was present in most afferent dendrites (Fig. 5). In cochleae from young rats (P9) $K_v$1.1-immunoreactivity was co-localized with many parvalbumin-positive dendritic terminals (Fig. 5A~D,


https://doi.org/10.5607/en22013

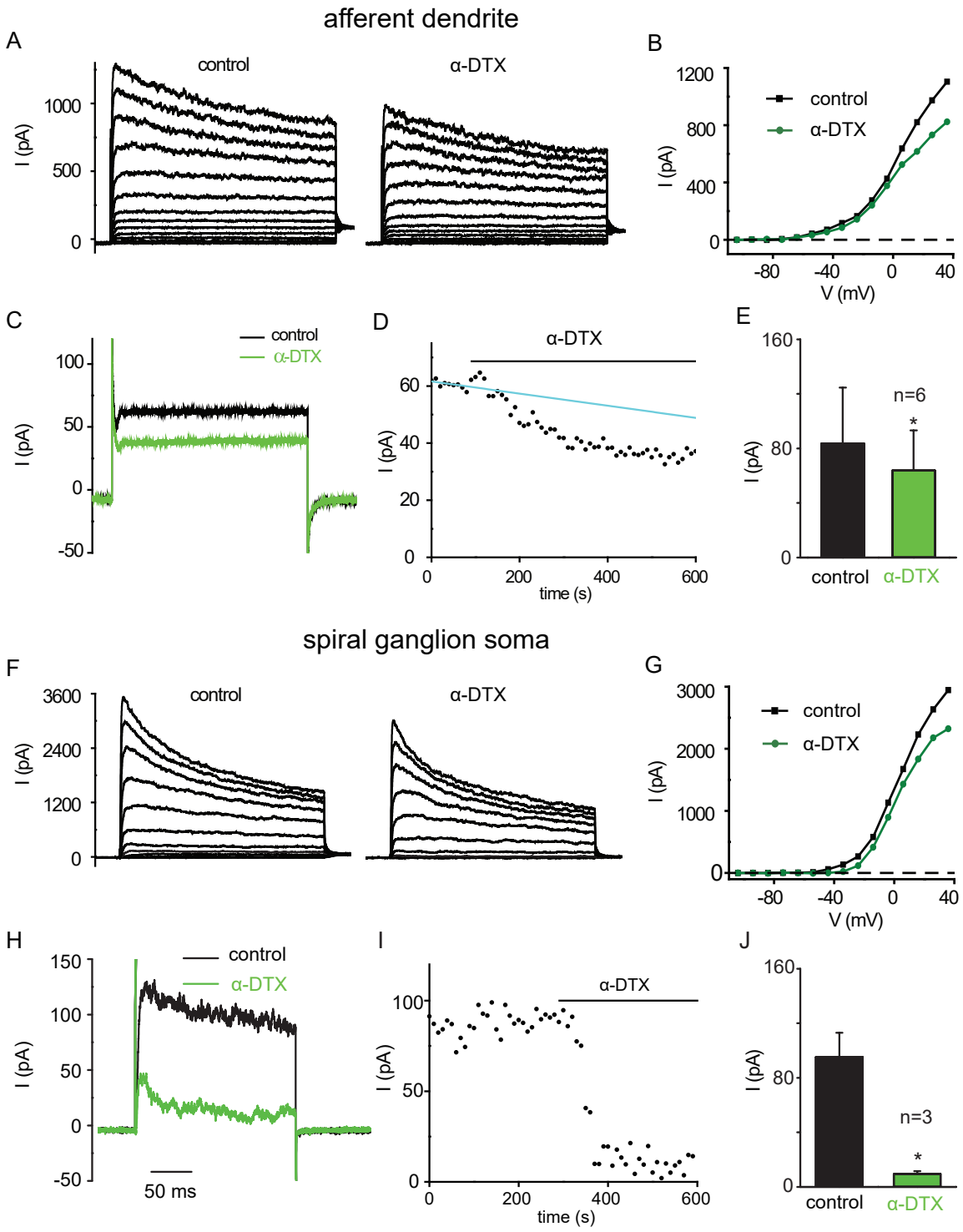


**Fig. 3.** Differential effect of α-dendrotoxin on $I_{KL}$ in the afferent dendrite versus the spiral ganglion soma. (A~D) ANF dendrite recording (7~14-day-old rat cochlea) before and during application of 100~200 nM α-DTX. (C) Current responses to 200 ms voltage steps from -84 to -34 mV before and during application of α-DTX (5 min). External solutions with TTX (1 μM), $CdCl_2$ (200 μM), ZD7288 (50 μM) and CNQX (10 μM). (D) Diary plot of the outward current measured at 20 ms into the voltage step; after leak subtraction. Rundown of the outward current was observed during recordings (fit by a line). Values extrapolated from this linear fit were used as control values for comparison to the current amplitudes in α-DTX. 27% of the outward current was inhibited by α-DTX in this recording. (E) Summarized results for 6 afferent dendrite recordings. (F~I) Spiral ganglion soma recording (1-day-old rat cochlea) before and during application of 200 nM α-DTX. (H) Current responses to voltage steps from -84 to -34 mV before and during application of α-DTX (5 min). (I) Diary plot of the outward current; after leak subtraction. There was no significant rundown in control. 88% of the outward current was blocked by α-DTX. (J) Summarized results for 3 spiral ganglion neuron soma recordings.

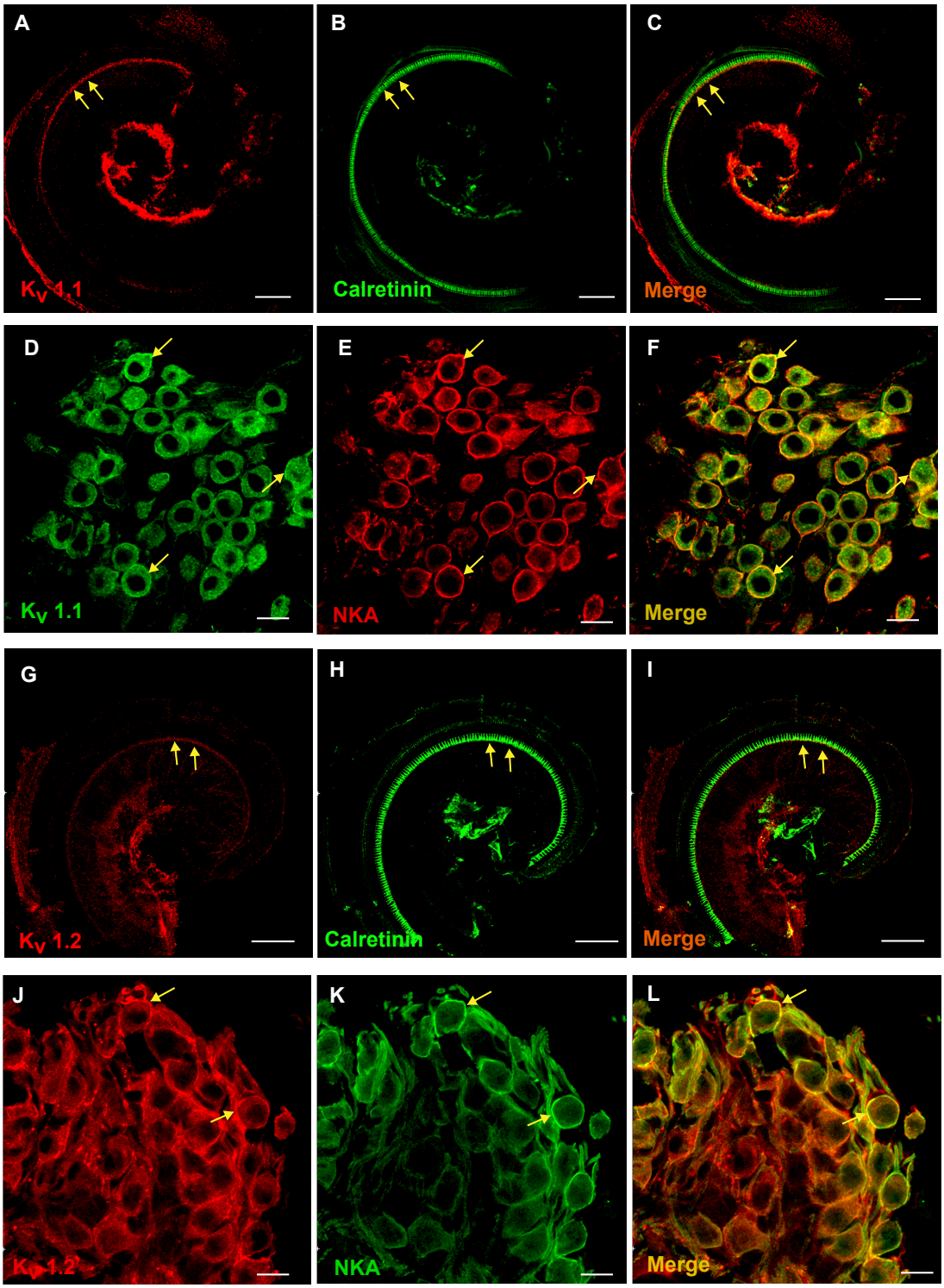


**Fig. 4.** $K_v$1.1 and $K_v$1.2-immunoreactivity in dendritic terminals and cell bodies of ANFs. (A~C) Low magnification confocal micrographs of whole-mount cochlear apical turn, double-labeled with anti-$K_v$1.1 (A, red) and anti-calretinin (B, green). $K_v$1.1 immunoreactivity is found near IHCs (yellow arrow) and in the spiral ganglion. Scale bar: 100 μm. (D~F) High-magnification confocal images of spiral ganglion. Double-labeling with a monoclonal anti- $K_v$1.1 (D, green) and anti-NKA (E, red) shows that $K_v$1.1 immunoreactivity is detected in the cell membranes and the cytosols of the majority of NKA-positive spiral ganglion cells. Scale bar: 10 μm. (G~I) Low magnification confocal micrographs of whole-mount cochlear apical turn, double-labeled with anti-$K_v$1.2 (G, red) and anti-calretinin (H, green). $K_v$1.2 immunoreactivity is found near IHCs (yellow arrow) and in the spiral ganglion. Scale bar: 150 μm. (J~L) High-magnification confocal images of spiral ganglion. Double-labeling with a monoclonal anti- $K_v$1.2 (J, red) and anti-NKA (K, green) shows that $K_v$1.2 immunoreactivity is detected in the cell membranes of the majority of NKA-positive spiral ganglion cells. Scale bar: 10 μm.


https://doi.org/10.5607/en22013

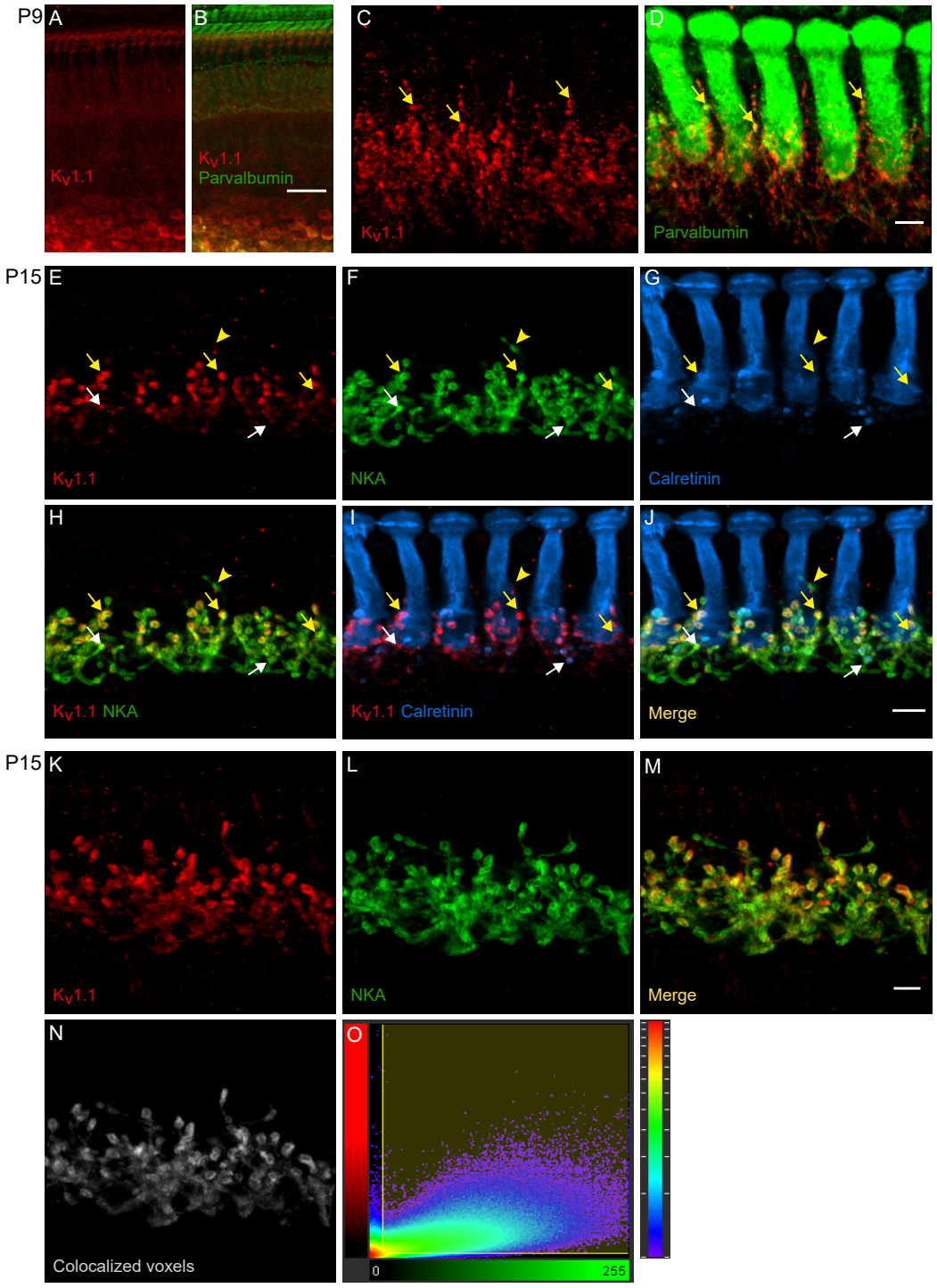


**Fig. 5.** Immunolabeling of $K_v1.1$ subunit in whole-mount cochlear preparations. (A, B) Low-magnification images of cochlear preparations (P9) double-labeled with anti-$K_v1.1$ (red) and anti-parvalbumin (green). Scale bar: 20 μm. (C, D) High-magnification images of cochlear preparations (P9) double-labeled with anti-$K_v1.1$ (red) and anti-parvalbumin (green). Scale bar: 5 μm. Yellow arrow: $K_v1.1$ and parvalbumin-positive terminals. (E~J) Confocal micrographs of cochlear preparations (P15) triple-labeled with anti-$K_v1.1$ (red), anti-NKA (green) and anti-calretinin (blue). $K_v1.1$ immunoreactivity is present in the majority of NKA and calretinin-positive dendritic terminals contacting onto inner hair cells. Yellow arrow: $K_v1.1$, NKA and calretinin-positive terminals. White arrow: $K_v1.1$ and NKA-positive but calretinin-negative terminals. Yellow arrowhead: NKA-positive but $K_v1.1$ negative terminals. Scale bar: 5 μm. (K~M) Maximum projection images from a confocal z stack show abundant $K_v1.1$ immunoreactivity in most NKA-positive dendritic segments. (N) Co-localized voxels exhibiting all co-localization result between $K_v1.1$ and NKA voxels. Scale bar: 5 μm. (O) 2D scatter plot of $K_v1.1$ and NKA-immunoreactivities. Scatter plot information on all the voxels was extracted from the same confocal 3D dataset depicted in K~M. Yellow vertical and horizontal lines indicate the background signals determined by automated threshold function in Imaris software.

yellow arrows). In cochleae from older hearing animals (P15~21) overall $K_v1.1$-immunoreactivity in afferent dendrites appeared stronger than in neonatal cochleae (Fig. 5E~J). Most NKA-immunolabeled and/or calretinin-immunolabeled dendritic terminals exhibited relatively intense $K_v1.1$-immunoreactivity (Fig. 5E~J, yellow or white arrows), while a small subset showed almost no $K_v1.1$-labeling (Fig. 5E~J, yellow arrowhead). An examination of z-stack projection images indicated that $K_v1.1$-immunoreactivity was present throughout the entire unmyelinated dendritic segments of most ANFs (Fig. 5K~M). $K_v1.1$ and NKA-immunoreactivities were highly correlated (Pearson's coefficient 0.7045) and 77% of NKA-immunoreactive voxels were $K_v1.1$-immnoreactive. Manders' coefficients calculated from this z-stack were 0.7991 (M1) and 0.5373 (M2), indicating high degree of co-localization of NKA- and $K_v1.1$-signals. Reconstructed images of $K_v1.1$ and NKA co-localized voxels (Fig. 3N) further emphasized a high degree of co-localization of $K_v1.1$- and NKA-immunoreactivity over the entire lengths of the dendritic segments, suggesting that $K_v1.1$ is located in most, but possibly not all afferent terminals.

$K_v1.2$-immunoreactivity had a similar labeling pattern compared to $K_v1.1$-immunoreactivity. At low magnification, strong signals were found in the IHC region and in the spiral ganglion region (Fig. 4G~L). In cochleae from young rats (P9) $K_v1.2$-immunoreactivity was found in many parvalbumin-positive dendritic terminals (Fig. 6A~D, yellow arrows). In cochleae from older rats (P15~21), the majority of dendritic terminals had $K_v1.2$-immunoreactivity (Fig. 6E~J, yellow arrows). As with $K_v1.1$-immunoreactivity, a minor subset of NKA and/or calretinin-positive dendritic terminals exhibited no $K_v1.2$-immunoreactivity (Fig. 6E~J, yellow arrowheads). Projection images of confocal z-stacks illustrated that $K_v1.2$-immunoreactivity was present along the entire unmyelinated segments (Fig. 6K~M). $K_v1.2$ and NKA-immunoreactivities were highly correlated (Pearson's coefficient 0.8004) and 79% of NKA-immunoreactive voxels were $K_v1.2$-immunoreactive. Manders' coefficients calculated from the z-stack images were 0.8568 (M1) and 0.7882 (M2), respectively. Occasionally, fibers projecting toward the OHC area exhibited $K_v1.2$-immunoreactivity (Fig. 6E~J, white arrowhead), but these fibers did not exhibit NKA- or calretinin-immunoreactivity. In the OHC area, NKA is expressed in efferent nerve fibers but not in type II ANFs [37]. Therefore, the $K_v1.2$-immunolabed fibers projecting toward the OHC area in our study were taken to be type II ANFs.

The z-stack projection images revealed uneven $K_v1.1$- and $K_v1.2$-immunoreactivity along the peripheral processes of ANFs (Fig. 7). Often, stronger labeling was found at the dendritic terminals and the small segments just below the habenular perforata (Fig. 7A~C), corresponding to the 2 peaks in the signal intensity plot (Fig. 7D, red trace). The $K_v1.1$-immunoreactivity below the habenular perforata corresponded well with Caspr-2-immunoreactivity, a marker for nodes of Ranvier, (Fig. 7E~H, dotted box), indicating that the lower $K_v1.1$-hot spots were probably at the first heminodes of the ANFs. $K_v1.2$-immunoreactivity exhibited a similar pattern, with the strongest signals near the dendritic terminals (Fig. 7I~L) and the first heminodes (Fig. 7M~P, dotted box).

Taken together, the prevalence, locations and signal intensities of $K_v1.1$ and $K_v1.2$ labeling implies a significant role of these subunits in modulating the excitability and AP generation at most IHC-ANF synapses.

### *The α-DTX-insensitive component of dendritic $I_{KL}$ is likely due to $K_v7.2$ and unknown subunits*

Although the immunolabeling results were consistent with the presence of α-DTX-sensitive $K^+$ channels in the majority of ANF dendrites, the electrophysiological evidence also indicated that a significant portion of dendritic $I_{KL}$ was mediated by α-DTX-insensitive $K^+$ channel subtype(s). Therefore, we performed immunolabeling studies with antibodies to non-$K_v1$ channels having significant open probabilities at negative membrane potentials. We chose to investigate $K_v7.2$ and $K_{2p}2.1$ because their expression had been previously reported in SGN somata and fiber-like structures near the base of the IHC [39]. In addition, $K_v7.2$ currents were reported to modify the resting membrane potentials and the excitabilities of isolated SGNs [40]. Indeed, $K_v7.2$-immunoreactivity can be found in SGN somata and some fiber-like structures near the bases of IHCs (Fig. 8A~F). However, co-labeling data with NKA demonstrated that not all of the $K_v7.2$-immunolabed fiber-like structures were ANF dendrites. Some $K_v7.2$-immunoreactivity was observed in the NKA-positive dendritic terminals (Fig. 8A~C, yellow arrows), while the presence of $K_v7.2$-immunoreactivity in NKA-negative structures (Fig. 8A~C, white arrows) was also clear. Most NKA-immunolabeled dendritic terminals showed no $K_v7.2$-immunoreactivity (Fig. 8A~C, white arrowheads). Taken together, these results indicated that $K_v7.2$ channels, although likely influencing $K^+$ current in most spiral ganglion somata, could contribute to $I_{KL}$ in only a subset of ANF dendrites.

$K_{2p}2.1$ is one of the $K^+$ "leak" channels helping to determine the resting membrane potential and input resistance of neurons. Within the inner ear, $K_{2p}2.1$-immunoreactivity has been observed in vestibular ganglion somata and vestibular afferent nerve terminals [41], and the presence of $K_{2p}2.1$ mRNA in mouse SGNs has been established [17]. In our experiments $K_{2p}2.1$-immunoreactivity was found in SGN somata (Fig. 8J~L) but not in ANF dendrites (Fig. 8G~I). Thus, the $K^+$ channel subtype(s) responsible for the α-DTX-insensitive component of dendritic $I_{KL}$ in rat ANFs remains to be


https://doi.org/10.5607/en22013

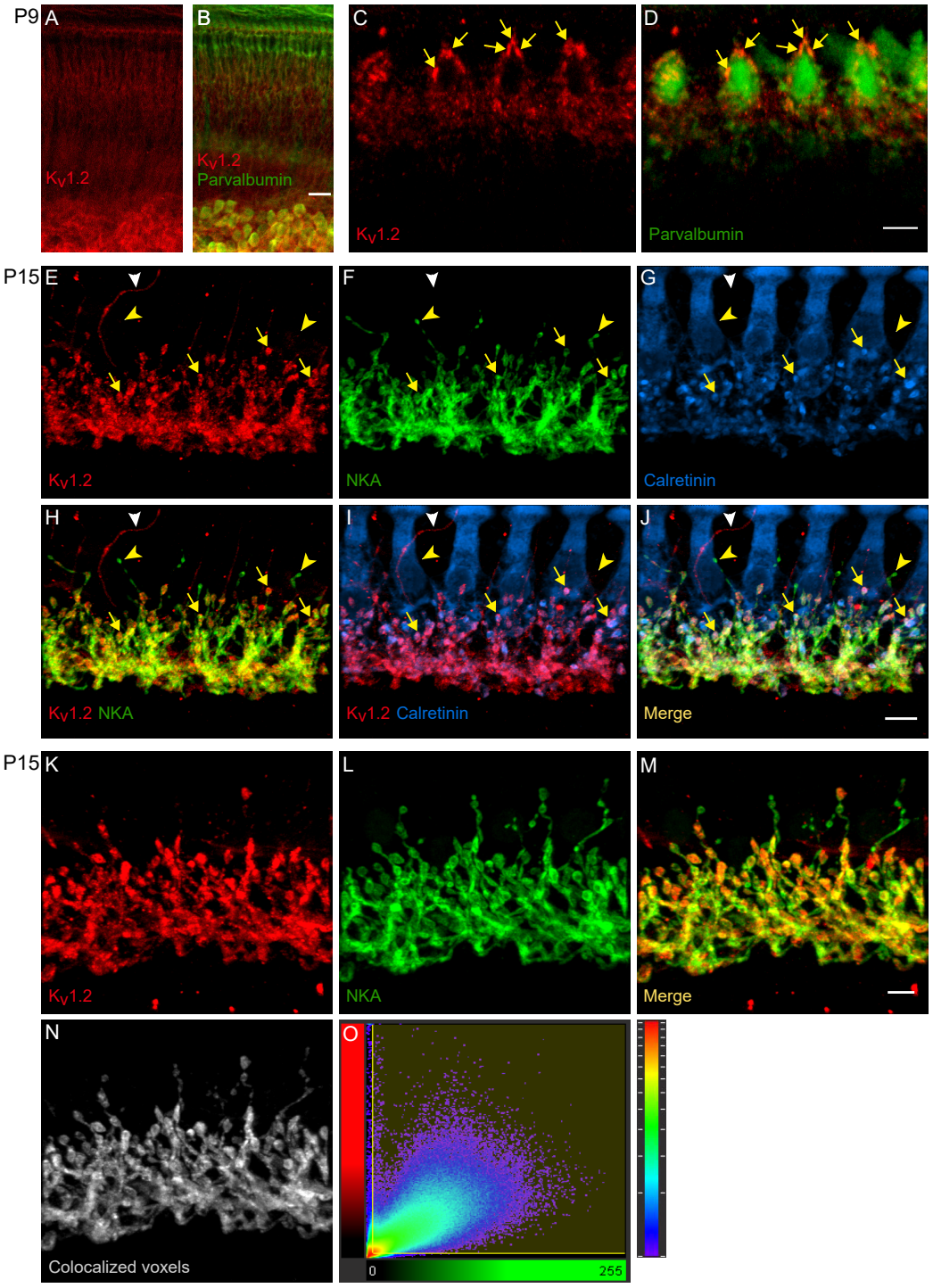


**Fig. 6.** Immunolabeling of $K_v1.2$ subunit in whole-mount cochlear preparations. (A, B) Low-magnification images of cochlear preparations (P9) double-labeled with anti-$K_v1.2$ (red) and anti-parvalbumin (green). Scale bar: 20 μm. (C, D) High-magnification images of cochlear preparations (P9 rat) double-labeled with anti-$K_v1.2$ (red) and anti-parvalbumin (green). Scale bar: 5 μm. yellow arrow: $K_v1.2$ and parvalbumin-positive terminals. (E~J) Confocal micrographs of cochlear preparations triple-labeled with anti-$K_v1.2$ (red), anti-NKA (green) and anti-calretinin (blue). $K_v1.2$ immunoreactivity is present in the majority of NKA and calretinin-positive dendritic terminals contacting onto inner hair cells. Yellow arrow: $K_v1.2$, NKA and calretinin-positive terminals. White arrowhead: fiber only positive for $K_v1.2$. yellow arrowhead: NKA-positive but $K_v1.2$- negative terminals. Scale bar: 5 μm. (K~M) Maximum projection images from a confocal z stack show abundant $K_v1.2$ immunoreactivity in most NKA-positive dendritic segments as well as the regions further along the nerve fibers. (N) Reconstructed image of voxels exhibiting both $K_v1.2$ and NKA signals. Scale bar: 5 μm. (O) 2D scatter plot of $K_v1.2$ and NKA-immunoreactivities. Scatter plot information on all the voxels was extracted from the same confocal 3D dataset depicted in K~M. Yellow vertical and horizontal lines indicate the background signals determined by automated threshold function in Imaris software.

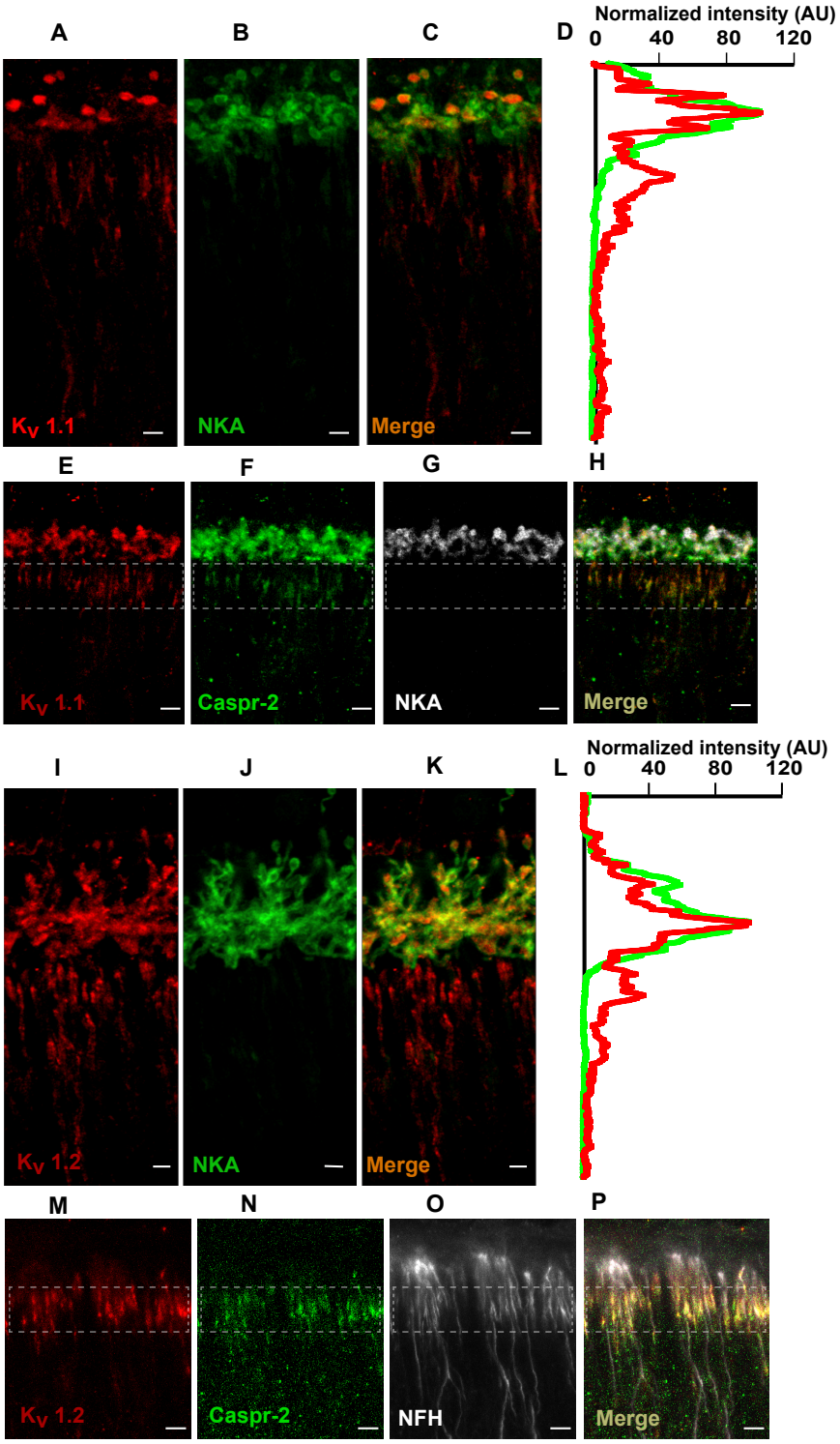


**Fig. 7.** $K_v$1.1 and $K_v$1.2 immunoreactivities are abundant at the first heminodes of ANFs. (A~C) Confocal micrographs of cochlear preparations double-labeled with anti-$K_v$1.1 (red), and anti-NKA (green). (D) Intensity profile of $K_v$1.1 and NKA-immunoreactivity along the length of peripheral process of ANF shown in A~C. (E~H) Confocal micrographs of cochlear preparations triple-labeled with anti-$K_v$1.1 (red), anti-NKA (grey) and anti-caspr-2 (green). (I~K) Confocal micrographs of cochlear preparations double-labeled with anti-$K_v$1.2 (red), and anti-NKA (green). (L) Intensity profile of $K_v$1.2 and NKA-immunoreactivity along the length of peripheral process of ANF shown in I~K. (M~P) Confocal micrographs of cochlear preparations triple-labeled with anti-$K_v$1.2 (red), anti-NFH (grey) and anti-caspr-2 (green). In addition to the high-intensity area at the dendritic segments, another signal peak was detected along the length of peripheral processes of ANFs. The second hot spots were found just below habenula perforata and corresponded well with Caspr-2 signals (dotted box in E~H and M~P). Scale bar: 5 μm.


https://doi.org/10.5607/en22013

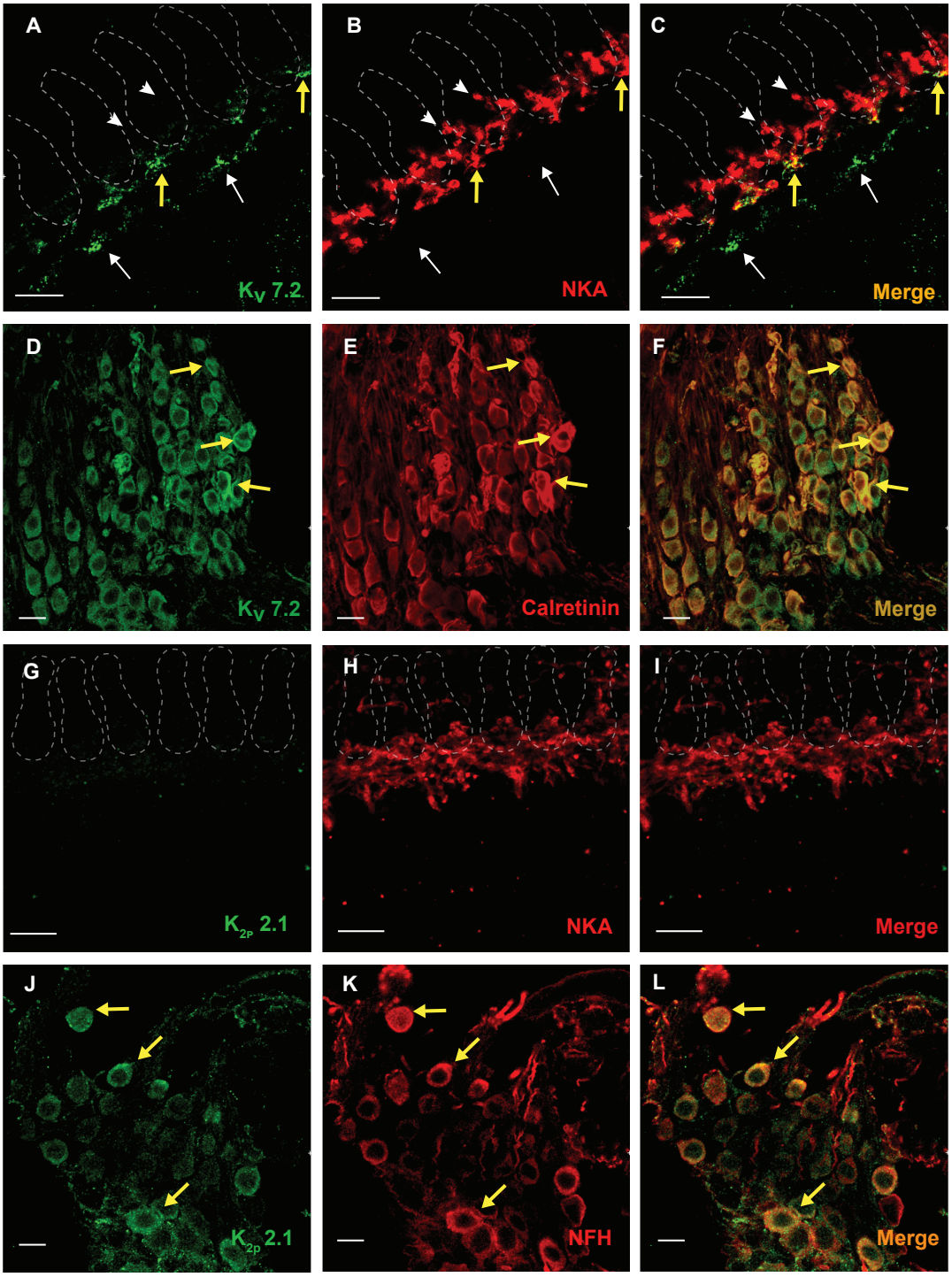


**Fig. 8.** Immunolabeling of $K_v7.2$ and $K_{2P}2.1$ subunits in whole-mount cochlear preparations. (A~C) Confocal images of cochlear turn double-labeled with anti-$K_v7.2$ (A, green) and anti-NKA (B, red). Outlines of IHCs are marked with dotted lines. Yellow arrow: $K_v7.2$ and NKA-positive dendritic terminals. White arrow: $K_v7.2$-positive but NKA-negative spots. White arrowhead: NKA-positive but $K_v7.2$-negative terminals. Scale bar: 10 μm. (D~F) Confocal images of spiral ganglion double-labeled with anti-$K_v7.2$ (D, green) and anti-calretinin (E, red). $K_v7.2$-immunoreactivity is detected in most calretinin-positive spiral ganglion somata (yellow arrow). Scale bar: 20 μm. (G~I) Confocal images of cochlear turn double-labeled with anti-$K_{2P}2.1$ (G, Green) and anti-NKA (H, red). Outlines of IHCs are marked with dotted lines. No $K_{2P}2.1$-immunoreactivity is detected at the NKA-positive dendritic terminals. Scale bar: 10 μm. (J~L) Confocal images of spiral ganglion double-labeled with anti-$K_{2P}2.1$ (J, green) and anti-NFH (K, red). $K_{2P}2.1$-immunoreactivity is detected in NFH-positive spiral ganglion somata (yellow arrow). Scale bar: 10 μm.

identified.

## DISCUSSION

ANF dendrites, similar to many auditory brainstem neurons, express 4-AP-sensitive $I_{KL}$ and 4-AP-resistant $I_{KH}$. In several classes of auditory brainstem neurons $I_{KL}$ is sensitive to dendrotoxins, and therefore it is most likely mediated by channels of the $K_v1$ family [2, 3, 25, 42-46]. Here, we found that the $I_{KL}$ of rat SGN somata is, in large part, α-DTX-sensitive, while that of ANF dendrites was only slightly sensitive to α-DTX. Similarly, the $I_{KL}$ of goldfish auditory afferent dendrites was 4-AP-sensitive and α-DTX–insensitive [47]. In the mammalian inner ear, 4-AP-sensitive but DTX-insensitive $I_{KL}$ has been found in vestibular calyx afferent terminals of the crista's peripheral zone [48]. Our immunolabeling data suggest the likely molecular makeup of rat dendritic low-threshold $K^+$ currents. First, our immunolabeling data indicate that the majority of afferent dendrites expresses $K_v1.1$- and $K_v1.2$-immunoreactivity, suggesting that $K_v1.1$ and $K_v1.2$ conduct $I_{KL}$ in most dendrites. The intensity of $K_v1.1$ and $K_v1.2$-immunoreactivity at the dendritic terminals was similarly strong as found at the heminodes although others have reported expression of $K_v1.1$ and $K_v1.2$ at the heminodes, nodes of Ranvier, and the SGN soma but not at the dendritic terminals of ANFs [32, 49]. We presume that the discrepancy at the dendritic terminals might be due to differences in the cochlear tissue preparations [32] or in the primary antibodies [49].

The $K^+$ channel(s) responsible for the α-DTX-resistant component of dendritic $I_{KL}$ remain to be identified. Possible candidates for the α-DTX-resistant component include $K_v1$ family subtypes known to be α-DTX insensitive ($K_v1.3$, 1.4, 1.5, 1.7, 1.8), or heteromeric $K^+$ channels containing $K_v1.1$ and $K_v1.2$ subunits. Although it has been generally thought that heteromeric $K^+$ channels containing at least one toxin-sensitive subunit exhibit toxin-sensitivity (single toxin-sensitive subunit model) [50], a recent study reported otherwise. In CHO cells expressing $K_v1.2$ and $K_v1.4$ subunits the heteromeric $K^+$ current was largely α-DTX-insensitive [19]. Our immunolabeling data also supported involvement of $K_v7.2$ channels in a small subset of dendrites. Similarly, Kim and Rutherford [49] reported $K_v7.2$ and $K_v7.3$ at the dendritic terminals of ANFs. Alternatively, based on their current-voltage profiles, members of the $K_v11$, $K_{ir}$, and $K_{2p}$ families of $K^+$ channels warrant future study.

There may be a functional advantage to the overlapping expression of different $K^+$ channel subtypes. Diverse dendritic ion channel expression might result from diverse olivocochlear (OC) efferent innervation during cochlear development and maturation. Indeed, evidence suggested that OC innervation influences the development of IHC-ANF synapse structure and function. Results from various transgenic mouse lines indicated that the coordination of $Ca^{2+}$ influx with glutamate release did not mature normally when efferent synaptic transmission to immature IHCs was disrupted during the early postnatal period [51, 52]. Moreover, surgical interruption of the OC fiber bundle disrupted both the pillar-modiolar gradient of the IHC ribbon structure, and the dendritic glutamate receptor patch size [53]. In addition, transgenic deletion of adenomatous polyposis coli protein from OC neurons [54] resulted in similar disruptions of the presynaptic ribbon structure and postsynaptic glutamate receptor patches.

Although the role and molecular identities of high-threshold dendritic $K^+$ channels were not investigated in great detail in this study, it is noteworthy that $I_{KH}$ could be activated by APs and in turn shape AP waveforms. $I_{KH}$ is mainly mediated by $K_v3$ channels in auditory brainstem neurons [55, 56]. Our group as well as others also have reported $K_v3.1b$ and $K_v3.3$ in dendrites and cell bodies of ANFs [24, 57]. Also, expression of $K_v3.1b$ had been demonstrated at the heminodes of ANFs [32, 49]. Thus, members of the $K_v3$ family are the most likely candidates for the dendritic channels mediating $I_{KH}$.

The firing of high frequency APs with minimal temporal variation is a common, critical property of auditory neurons, and $I_{KL}$, conducted primarily by the $K_v1$ family of channels, helps the temporal precision of this firing. For example, auditory neurons from animals lacking $K_v1.1$ exhibited abnormally low $I_{KL}$, and performed poorly in auditory tasks requiring high temporal precision of signaling [58, 59]. At the cellular level, pharmacological antagonism or genetic deletion of $K_v1.1$ in auditory brainstem neurons caused 1) increased AP jitter, 2) decreased fidelity of input/output rates during stimulus trains, and 3) reduced phase-locked firing in response to sinusoidal sound stimuli [60-62]. In these neurons, $I_{KL}$ helped maintain low $R_{in}$, and thereby shortened the durations of EPSPs and APs. Similarly, our results indicated that $I_{KL}$ of ANF dendrites, especially those conducted by $K_v1.1$ and/or $K_v1.2$, played a significant role in shortening dendritic EPSPs. It is possible that the observed shortening of EPSP durations (~22%) could have an even greater effect *in vivo*, since ANF dendrites express another voltage-sensitive current whose activity can be triggered by $I_{KL}$. ANF dendrites express $I_h$ that exhibited 3~9% open probability at -65 mV [21], and depolarized the membrane to potentials where more $I_{KL}$ increases. Conversely, increased $I_{KL}$ hyperpolarized the membrane potential, increasing $I_h$. Thus, $I_h$ and $I_{KL}$ work in concert to dramatically decrease $R_{in}$ without changing resting membrane potential. Indeed, such synergistic effects of $I_h$ and $I_{KL}$ in decreasing $R_{in}$ and EPSP duration has been demonstrated in medial superior olive neurons [1], and in a computational model of ventral cochlear nucleus neurons [63]. Another factor to consider is that our data


https://doi.org/10.5607/en22013

were recorded from neonatal rat cochleae at room temperature. The size of $I_{KL}$ might undergo a developmental increase during the first 3~4 postnatal weeks, as reported in medial superior olive neurons [8], and $I_{KL}$ amplitudes have also been shown to increase with increasing temperature [64].

In addition to shortening EPSP durations, $K_v1$ currents directly modulate AP generation in ANFs. In isolated SGN somata with severed axonal and dendritic processes, blocking $I_{KL}$ with dendrotoxins significantly decreased AP thresholds and altered firing pattern from rapidly adapting to slowly adapting type [18-20]. Immunolabeling presented here and by others [32, 49, 65], demonstrate a presence of $K_v1.1$ and $K_v1.2$ hot spots at the first heminodes of ANFs, provided further evidence for the involvement of $K_v1$ in AP generation at the AP initiation zone.

Taken together, our data suggest that $K_v1.1$- and $K_v1.2$-containing $K^+$ channels improve temporal resolution at the IHC-ANF synapse by directly shortening EPSPs at the synapse and modulating AP generation at the first node of ANFs.

## ACKNOWLEDGEMENTS

Authors appreciate Dr. Jeffrey A. Love for critically reading the manuscript and Dr. Sung Hwa Hong for his critical comments.

This work was supported by Basic Science Research Program through the National Research Foundation of Korea (NRF) funded by the Ministry of Education (2019R1I1A3A01063625, to EY); National Institute on Deafness and Other Communication Disorders grants (R01DC006476 and R01DC012957 to EG); the David M. Rubenstein Fund for Hearing Research and the John Mitchell Jr. Trust.

## AUTHOR CONTRIBUTIONS

EG and EY conceived the idea, designed the experiments. KS, KK, YS, and EY performed the immunolabeling experiments and data analysis. All authors contributed to preparation of the initial draft. EY performed electrophysiological recordings, and supervised the project.

## REFERENCES

1. Mathews PJ, Jercog PE, Rinzel J, Scott LL, Golding NL (2010) Control of submillisecond synaptic timing in binaural coincidence detectors by K(v)1 channels. Nat Neurosci 13:601-609.
2. Bal R, Oertel D (2001) Potassium currents in octopus cells of the mammalian cochlear nucleus. J Neurophysiol 86:2299-2311.
3. Brew HM, Forsythe ID (1995) Two voltage-dependent K+ conductances with complementary functions in postsynaptic integration at a central auditory synapse. J Neurosci 15:8011-8022.
4. Dodson PD, Forsythe ID (2004) Presynaptic K+ channels: electrifying regulators of synaptic terminal excitability. Trends Neurosci 27:210-217.
5. Macica CM, von Hehn CA, Wang LY, Ho CS, Yokoyama S, Joho RH, Kaczmarek LK (2003) Modulation of the kv3.1b potassium channel isoform adjusts the fidelity of the firing pattern of auditory neurons. J Neurosci 23:1133-1141.
6. Middlebrooks JC, Nick HS, Subramony SH, Advincula J, Rosales RL, Lee LV, Ashizawa T, Waters MF (2013) Mutation in the kv3.3 voltage-gated potassium channel causing spinocerebellar ataxia 13 disrupts sound-localization mechanisms. PLoS One 8:e76749.
7. Nakamura Y, Takahashi T (2007) Developmental changes in potassium currents at the rat calyx of Held presynaptic terminal. J Physiol 581(Pt 3):1101-1112.
8. Scott LL, Mathews PJ, Golding NL (2005) Posthearing developmental refinement of temporal processing in principal neurons of the medial superior olive. J Neurosci 25:7887-7895.
9. Bortone DS, Mitchell K, Manis PB (2006) Developmental time course of potassium channel expression in the rat cochlear nucleus. Hear Res 211:114-125.
10. Berglund AM, Ryugo DK (1987) Hair cell innervation by spiral ganglion neurons in the mouse. J Comp Neurol 255:560-570.
11. Goutman JD, Glowatzki E (2007) Time course and calcium dependence of transmitter release at a single ribbon synapse. Proc Natl Acad Sci U S A 104:16341-16346.
12. Grant L, Yi E, Glowatzki E (2010) Two modes of release shape the postsynaptic response at the inner hair cell ribbon synapse. J Neurosci 30:4210-4220.
13. Hossain WA, Antic SD, Yang Y, Rasband MN, Morest DK (2005) Where is the spike generator of the cochlear nerve? Voltage-gated sodium channels in the mouse cochlea. J Neurosci 25:6857-6868.
14. Rutherford MA, Chapochnikov NM, Moser T (2012) Spike encoding of neurotransmitter release timing by spiral ganglion neurons of the cochlea. J Neurosci 32:4773-4789.
15. Glowatzki E, Fuchs PA (2002) Transmitter release at the hair cell ribbon synapse. Nat Neurosci 5:147-154.
16. Adamson CL, Reid MA, Mo ZL, Bowne-English J, Davis RL (2002) Firing features and potassium channel content of murine spiral ganglion neurons vary with cochlear location. J

Comp Neurol 447:331-350.
17. Chen WC, Davis RL (2006) Voltage-gated and two-pore-domain potassium channels in murine spiral ganglion neurons. Hear Res 222:89-99.
18. Liu Q, Lee E, Davis RL (2014) Heterogeneous intrinsic excitability of murine spiral ganglion neurons is determined by Kv1 and HCN channels. Neuroscience 257:96-110.
19. Wang W, Kim HJ, Lv P, Tempel B, Yamoah EN (2013) Association of the Kv1 family of K+ channels and their functional blueprint in the properties of auditory neurons as revealed by genetic and functional analyses. J Neurophysiol 110:1751-1764.
20. Mo ZL, Adamson CL, Davis RL (2002) Dendrotoxin-sensitive K(+) currents contribute to accommodation in murine spiral ganglion neurons. J Physiol 542(Pt 3):763-778.
21. Yi E, Roux I, Glowatzki E (2010) Dendritic HCN channels shape excitatory postsynaptic potentials at the inner hair cell afferent synapse in the mammalian cochlea. J Neurophysiol 103:2532-2543.
22. Grant L, Yi E, Goutman JD, Glowatzki E (2011) Postsynaptic recordings at afferent dendrites contacting cochlear inner hair cells: monitoring multivesicular release at a ribbon synapse. J Vis Exp 48:2442.
23. Sharma K, Seo YW, Yi E (2018) Differential expression of $Ca^{2+}$-buffering protein calretinin in cochlear afferent fibers: a possible link to vulnerability to traumatic noise. Exp Neurobiol 27:397-407.
24. Kim WB, Kang KW, Sharma K, Yi E (2020) Distribution of Kv3 subunits in cochlear afferent and efferent nerve fibers implies distinct role in auditory processing. Exp Neurobiol 29:344-355.
25. Cao XJ, Shatadal S, Oertel D (2007) Voltage-sensitive conductances of bushy cells of the mammalian ventral cochlear nucleus. J Neurophysiol 97:3961-3975.
26. Rothman JS, Manis PB (2003) Differential expression of three distinct potassium currents in the ventral cochlear nucleus. J Neurophysiol 89:3070-3082.
27. Brew HM, Forsythe ID (2005) Systematic variation of potassium current amplitudes across the tonotopic axis of the rat medial nucleus of the trapezoid body. Hear Res 206:116-132.
28. Zhang S, Trussell LO (1994) A characterization of excitatory postsynaptic potentials in the avian nucleus magnocellularis. J Neurophysiol 72:705-718.
29. Golding NL, Robertson D, Oertel D (1995) Recordings from slices indicate that octopus cells of the cochlear nucleus detect coincident firing of auditory nerve fibers with temporal precision. J Neurosci 15:3138-3153.
30. Banks MI, Smith PH (1992) Intracellular recordings from neurobiotin-labeled cells in brain slices of the rat medial nucleus of the trapezoid body. J Neurosci 12:2819-2837.
31. Harvey AL, Robertson B (2004) Dendrotoxins: structure-activity relationships and effects on potassium ion channels. Curr Med Chem 11:3065-3072.
32. Smith KE, Browne L, Selwood DL, McAlpine D, Jagger DJ (2015) Phosphoinositide modulation of heteromeric Kv1 channels adjusts output of spiral ganglion neurons from hearing mice. J Neurosci 35:11221-11232.
33. Petitpré C, Wu H, Sharma A, Tokarska A, Fontanet P, Wang Y, Helmbacher F, Yackle K, Silberberg G, Hadjab S, Lallemend F (2018) Neuronal heterogeneity and stereotyped connectivity in the auditory afferent system. Nat Commun 9:3691.
34. Shrestha BR, Chia C, Wu L, Kujawa SG, Liberman MC, Goodrich LV (2018) Sensory neuron diversity in the inner ear is shaped by activity. Cell 174:1229-1246.e17.
35. Sun S, Babola T, Pregernig G, So KS, Nguyen M, Su SM, Palermo AT, Bergles DE, Burns JC, Müller U (2018) Hair cell mechanotransduction regulates spontaneous activity and spiral ganglion subtype specification in the auditory system. Cell 174:1247-1263.e15.
36. Dechesne CJ, Winsky L, Kim HN, Goping G, Vu TD, Wenthold RJ, Jacobowitz DM (1991) Identification and ultrastructural localization of a calretinin-like calcium-binding protein (protein 10) in the guinea pig and rat inner ear. Brain Res 560:139-148.
37. McLean WJ, Smith KA, Glowatzki E, Pyott SJ (2009) Distribution of the Na,K-ATPase alpha subunit in the rat spiral ganglion and organ of corti. J Assoc Res Otolaryngol 10:37-49.
38. Kujawa SG, Liberman MC (2009) Adding insult to injury: cochlear nerve degeneration after "temporary" noise-induced hearing loss. J Neurosci 29:14077-14085.
39. Jin Z, Liang GH, Cooper EC, Jarlebark L (2009) Expression and localization of K channels KCNQ2 and KCNQ3 in the mammalian cochlea. Audiol Neurootol 14:98-105.
40. Lv P, Wei D, Yamoah EN (2010) Kv7-type channel currents in spiral ganglion neurons: involvement in sensorineural hearing loss. J Biol Chem 285:34699-34707.
41. Popper P, Winkler J, Erbe CB, Lerch-Gaggl A, Siebeneich W, Wackym PA (2008) Distribution of two-pore-domain potassium channels in the adult rat vestibular periphery. Hear Res 246:1-8.
42. Dodson PD, Billups B, Rusznák Z, Szûcs G, Barker MC, Forsythe ID (2003) Presynaptic rat Kv1.2 channels suppress synaptic terminal hyperexcitability following action potential

invasion. J Physiol 550(Pt 1):27-33.
43. Barnes-Davies M, Barker MC, Osmani F, Forsythe ID (2004) Kv1 currents mediate a gradient of principal neuron excitability across the tonotopic axis in the rat lateral superior olive. Eur J Neurosci 19:325-333.
44. Leao RN, Berntson A, Forsythe ID, Walmsley B (2004) Reduced low-voltage activated K+ conductances and enhanced central excitability in a congenitally deaf (dn/dn) mouse. J Physiol 559(Pt 1):25-33.
45. Lu Y, Monsivais P, Tempel BL, Rubel EW (2004) Activity-dependent regulation of the potassium channel subunits Kv1.1 and Kv3.1. J Comp Neurol 470:93-106.
46. Oertel D, Shatadal S, Cao XJ (2008) In the ventral cochlear nucleus Kv1.1 and subunits of HCN1 are colocalized at surfaces of neurons that have low-voltage-activated and hyperpolarization-activated conductances. Neuroscience 154:77-86.
47. Curti S, Gómez L, Budelli R, Pereda AE (2008) Subthreshold sodium current underlies essential functional specializations at primary auditory afferents. J Neurophysiol 99:1683-1699.
48. Meredith FL, Rennie KJ (2015) Zonal variations in K+ currents in vestibular crista calyx terminals. J Neurophysiol 113:264-276.
49. Kim KX, Rutherford MA (2016) Maturation of NaV and KV channel topographies in the auditory nerve spike initiator before and after developmental onset of hearing function. J Neurosci 36:2111-2118.
50. Hopkins WF (1998) Toxin and subunit specificity of blocking affinity of three peptide toxins for heteromultimeric, voltage-gated potassium channels expressed in Xenopus oocytes. J Pharmacol Exp Ther 285:1051-1060.
51. Johnson SL, Wedemeyer C, Vetter DE, Adachi R, Holley MC, Elgoyhen AB, Marcotti W (2013) Cholinergic efferent synaptic transmission regulates the maturation of auditory hair cell ribbon synapses. Open Biol 3:130163.
52. Johnson SL, Kuhn S, Franz C, Ingham N, Furness DN, Knipper M, Steel KP, Adelman JP, Holley MC, Marcotti W (2013) Presynaptic maturation in auditory hair cells requires a critical period of sensory-independent spiking activity. Proc Natl Acad Sci U S A 110:8720-8725.
53. Yin Y, Liberman LD, Maison SF, Liberman MC (2014) Olivocochlear innervation maintains the normal modiolar-pillar and habenular-cuticular gradients in cochlear synaptic morphology. J Assoc Res Otolaryngol 15:571-583.
54. Hickman TT, Liberman MC, Jacob MH (2015) Adenomatous polyposis coli protein deletion in efferent olivocochlear neurons perturbs afferent synaptic maturation and reduces the dynamic range of hearing. J Neurosci 35:9236-9245.
55. Perney TM, Kaczmarek LK (1997) Localization of a high threshold potassium channel in the rat cochlear nucleus. J Comp Neurol 386:178-202.
56. Song P, Yang Y, Barnes-Davies M, Bhattacharjee A, Hamann M, Forsythe ID, Oliver DL, Kaczmarek LK (2005) Acoustic environment determines phosphorylation state of the Kv3.1 potassium channel in auditory neurons. Nat Neurosci 8:1335-1342.
57. Bakondi G, Pór A, Kovács I, Szucs G, Rusznák Z (2008) Voltage-gated K+ channel (Kv) subunit expression of the guinea pig spiral ganglion cells studied in a newly developed cochlear free-floating preparation. Brain Res 1210:148-162.
58. Allen PD, Ison JR (2012) Kcna1 gene deletion lowers the behavioral sensitivity of mice to small changes in sound location and increases asynchronous brainstem auditory evoked potentials but does not affect hearing thresholds. J Neurosci 32:2538-2543.
59. Karcz A, Allen PD, Walton J, Ison JR, Kopp-Scheinpflug C (2015) Auditory deficits of Kcna1 deletion are similar to those of a monaural hearing impairment. Hear Res 321:45-51.
60. Brew HM, Hallows JL, Tempel BL (2003) Hyperexcitability and reduced low threshold potassium currents in auditory neurons of mice lacking the channel subunit Kv1.1. J Physiol 548(Pt 1):1-20.
61. Gittelman JX, Tempel BL (2006) Kv1.1-containing channels are critical for temporal precision during spike initiation. J Neurophysiol 96:1203-1214.
62. Kopp-Scheinpflug C, Fuchs K, Lippe WR, Tempel BL, Rübsamen R (2003) Decreased temporal precision of auditory signaling in Kcna1-null mice: an electrophysiological study in vivo. J Neurosci 23:9199-9207.
63. Rothman JS, Manis PB (2003) The roles potassium currents play in regulating the electrical activity of ventral cochlear nucleus neurons. J Neurophysiol 89:3097-3113.
64. Cao XJ, Oertel D (2005) Temperature affects voltage-sensitive conductances differentially in octopus cells of the mammalian cochlear nucleus. J Neurophysiol 94:821-832.
65. Lacas-Gervais S, Guo J, Strenzke N, Scarfone E, Kolpe M, Jahkel M, De Camilli P, Moser T, Rasband MN, Solimena M (2004) BetaIVSigma1 spectrin stabilizes the nodes of Ranvier and axon initial segments. J Cell Biol 166:983-990.